The University of Akron
IdeaExchange@UAkron

Honors Research Projects

The Dr. Gary B. and Pamela S. Williams Honors College

Spring 2016

Passivation and Potential Fluctuation of AZ31B Alloy in Alkaline Environments

Ana C. Bacco
The University of Akron, acb70@zips.uakron.edu

Passivation and Potential Fluctuation of AZ31B Alloy in Alkaline Environments

4250:497

Honors Advisor

Dr. Hongbo Cong

Honors Project Advisor

Dr. Hongbo Cong

Readers

Dr. Rajeev Gupta

Dr. Qixin Zhou

Author

Ana Bacco

Date

4/08/2016

Executive Summary

Purpose

Magnesium (Mg) alloys are used in many different industries because of their low density, high thermal conductivity, and their comparable strength to weight ratio to aluminum. On the other hand, Mg alloys have high chemical reactivity and poor oxide film protection which makes them inferior to other alloys. The purpose of this project was to investigate the potential fluctuation of Mg alloy AZ31B in alkaline environments. Potential fluctuation indicates passivation/corrosion activity occurring in the Mg alloy. This project focused on identifying possible causes for the potential fluctuations of AZ31B in alkaline environments. By studying Mg alloys in alkaline environments, a higher understanding for anodization and self-healing metallic coatings before application. The mechanisms behind passivation can be analyzed in order to determine the strengths and weaknesses to enhance the material. Mg anodization improves its corrosion resistance and allows for broader industrial use. Mg's lightweight, reduced cost, and lower environmental hazards when die casting as compared to aluminum are factors which industries find attractive[1]. Companies working within the automotive industry would exploit these properties in order to gain a competitive advantages with their fuel efficiencies and environmentally friendlier processes.

Findings and Results

Electrochemical experiments and surface characterization allowed for several findings and results on microstructure, corrosion morphology, effects of oxygen, pH and also allowed for theories on the passivation mechanisms of AZ31B in alkaline solutions. AZ31B contains two intermetallic particles (IMPs) that are composed of aluminum-manganese (Al-Mn) and aluminum-zinc (Al-Zn) IMPs (Figure 1). Potential fluctuations were identified for both long and short term immersion in 1 M NaOH (Figure 2). After immersion, it was found that smaller Al-Mn IMPs completely dissolved and larger IMPs partially dissolved. The partially dissolved Al-Mn IMPs developed an oxide film overtop. Al-Zn IMPs however,

did not dissolve under these conditions (Figure 3).The formation of oxide nodules were also found at the interface of α-Mg phase and the β-phase. Nodules developed cracks due to increased volume (Figure 7).

Under deaerated conditions in 1 M NaOH, the magnitude and the frequency of the potential fluctuations significantly decreased as compared to static conditions (Figure 8). Surface characterization revealed that Al-Mn IMPs significantly dissolved and only a thin oxide film developed (Figure 9).

Potential measurements changed based on the pH level of the NaOH solution. Significant potential drops occurred in pH 13 and 14, but not under pH 10, 11, nor 12 (Figure 10). Surface characterization revealed oxide domes that formed overtop the Al-Mn particles with severe corrosion occurring on the α-Mg phase in pH 11 conditions. After pH 12 immersion, AZ31B showed less significant corrosion/passivation on the surface (Figure 12). Cathodic activities were also tested in order to understand the corrosion/passivation activities of AZ31B when immersed in different pH levels in static conditions. Through immersion testing and live visual inspection, it was seen that pH level 11 showed the most significant bubble formation activity. At pH 12 however, minimal bubble formation was seen. At pH 13 and 14, the initial bubble formation decreased with time (Figure 15).

Discussion

The cracking that occurred can be a possible explanation for the potential drops seen in the open circuit potential measurements. Stressed developed cracks expose fresh magnesium surface to the solution, which oxidizes and creates oxide nodules. The newly exposed magnesium causes the potential reading recorded to drop back down to the active state (i.e., ~ -1.6 V_{SCE}). By testing AZ31B under deaerated conditions it was found its potential stabilized around -1.3 V_{SCE} with potential drops continuing to occur. From this, it can be deduced that the oxygen reduction reaction was responsible for increasing the potential and stabilizing it in the passive state (i.e., -0.4 – -0.6 V_{SCE}).

The cathodic activities occurring on the surface of AZ31B in addition to the surface characterization that was done previously lead to possible mechanisms that may be occurring that are related to galvanic

activities between the Al-Mn IMPs and the α-Mg matrix. Under pH 10 and 11 environments the Al-Mn IMPs did not dissolve and oxide domes formed overtop. This indicates that the Al-Mn IMPs act as the cathodes and the α-Mg matrix act as the anodes therefore, the Al-Mn IMPs support the cathodic reactions allowing hydrogen bubbles to form overtop of the IMPs (Figure 18). Under pH 13 and 14, the Al-Mn IMPs dissolved with time and an oxide film formed overtop protecting the IMPs from further dissolving. The fact that the Al-Mn IMPs initially dissolved indicates that they are the anodes under these pH levels and the adjacent α-Mg matrix acts as the cathode. The cathodic reaction is now supported by α-Mg matrix therefore, it is theorized that the bubble formation is occurring at the interface of the Al-Mn IMPs and α-Mg matrix due to the galvanic interactions between the Al-Mn IMPs and α-Mg matrix (Figure 19). Notice that the majority of the α-Mg matrix also act as anode in the strongly alkaline solutions (pH = 13 and 14).

Implications of Work

These results can benefit society because they introduce new ideas and approaches that can be applied to different materials such as, metals and coatings. By increasing knowledge of corrosion/passivation behavior, we can learn how to apply or approach different problems. This work taught me laboratory corrosion testing techniques that are important when selecting a material. These techniques allow you to simulate different environments that your material may or will be exposed to. Scanning electron microscope and optical microscope are surface characterization techniques that are also important to perform when choosing a material and understanding corrosion behavior. Presenting a technical symposium at the National Association of Corrosion Engineers (NACE) also prepared me for future career presentations by enhancing my technical, soft, self-confidence, and presenting skills.

Recommendations

My recommendation would be to attempt to model the corrosion/passivation on a software by firstly beginning with Corrosion Master. This would then help into making a model simulation. My recommendation to students that work on similar projects is to ask questions and to not be afraid to ask

for help or further explanation. I would recommend that they think outside the box and think of experiences or classes they have taken that can relate back to their project.

Introduction

The purpose of this project was to investigate the passivation and potential fluctuation of AZ31B magnesium alloy in alkaline environments. The Department of Defense, automotive, aerospace, and many other industries are interested in magnesium alloys due to their light density, their strength-weight, and stiffness-weight ratios as compared to steel and aluminum alloys. Magnesium alloys however, are inferior due to their high chemical reactivity and poor oxide film protection. Therefore, it is crucial to understand the corrosion mechanisms and behaviors that occur within magnesium and magnesium alloys in order to replace aluminum alloys and steel with this material. The use of this material can for example, create more fuel efficient vehicles as well as improve many other products while still maintaining integrity and reliability of the metal.

Sample preparation for AZ31B will include the cutting and polishing of the AZ31. The alloy will be submerged in varying pH NaOH solutions at ambient temperature as well as, under static and deaerated conditions. A three-electrode-configuration flat cell equipped with a flush mount as the working electrode, a niobium platinum mesh as the counter, and a saturated calomel electrode as the reference electrode was used in order to perform open circuit potential measurements as well as, cyclic potentiodynamic polarization tests. The investigation included the surface characterization of the magnesium alloys after exposure using an optical microscope and a field emission scanning electron microscope equipped with a gallium focused beam. This analysis was done in order to investigate 1) the oxide film formation and rupture in chloride free alkaline solutions, 2) the effects of oxygen and solution pH on the passivation/corrosion of AZ31B, and 3) correlate the secondary phases and intermetallic particles on the oxidation and corrosion behavior of AZ31B in alkaline solutions.

Background

Magnesium (Mg) and Mg alloys passivate in alkaline solutions and corrode in more neutral and acidic environments[2]. The passive film that is formed on the surface of the alloy in alkaline solutions is reported to be composed of $Mg(OH)_2$ and an MgO inner layer[2]. Despite the passive film formation that increase open circuit potential (OCP), it has been seen that magnesium alloys experience potential fluctuations. The open circuit potential fluctuates between approximately -1.6 V_{SCE} and -0.5 V_{SCE}. These fluctuations were said to be a result of passive film ruptures that expose the material causing the potential to drop[3]. Moreover, magnesium alloys contain intermetallic particles (IMPs) that have galvanic interactions with the alloys secondary phases. This however, has not been studied thus far in alkaline environments. For this reason, this project focused on the IMPs effect on corrosion/passivation behavior in order to understand the activity of AZ31B in alkaline environments. This research will shed light on magnesium surface pre-treatments before the development of conversion coatings on them.

Experimental Methods

Samples of AZ31B were cut into $25 \times 25 \times 3$ and grinded using 600 grit sand paper with ethanol. After grinding and cleaning, the samples were then polished successively with 9 μm, 3 μm, and 1 μm oil based diamond slurries. In order to analyze the microstructure of AZ31B, the samples were etched with Acetic-Picral (5 g picric acid, 5 ml acetic acid, 10 ml H_2O, and 100 ml ethanol).

Electrochemical tests and scanning vibrating electrode techniques (SVET) were performed of the AZ31B samples. Field emission scanning electron microscope (FE-SEM) with a gallium focused ion beam (FIB) and energy dispersive spectroscopy (EDS) were used in order to analyze the surface and microstructure of AZ31B. A three-electrode-configuration flat cell was used for the electrochemical portion of this investigation. A flush mount was used as the working electrode, while a platinum niobium mesh was used as the counter electrode. A saturated calomel electrode was used as the reference for the experiments. Sodium hydroxide (NaOH) was the electrolyte of choice for this research and the pH levels ranged from 10 – 14. Static and deaerated conditions were also studied in this investigation where Argon (99.998%) was used for the deaeration process. Open circuit potential and cyclic potentiodynamic polarization

measurements were the electrochemical tests that were performed.

Data and Results

The microstructure of AZ31B contains an α-Mg matrix and a β-phase. Two types of IMPs were also identified within the alloy. Aluminum manganese (Al-Mn) IMP shown as a1 and an aluminum zinc (Al-Zn) IMP labeled as a2 in Figure 1a. Figure b shows that Al-Zn particles are found within the β-phase, while Al-Mn particles are isolated in the α-Mg matrix. The compositions of the IMPs can be seen in Table 1.
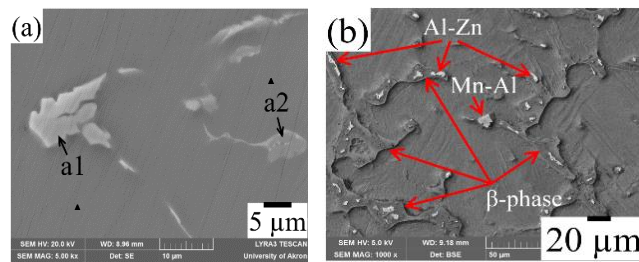

Figure 1: AZ31B microstructure showing a) the Al-Mn and Al-Zn IMPs and b) the secondary phases and placement of the IMPS.

Table 1: Elemental compositions (at.%) of AZ31B IMPs.

IMPs	Mg	Al	Zn	Mn	Fe
a$_1$	3.30	**39.84**	-	**55.19**	1.66
a$_2$	69.06	**23.67**	**7.26**	-	-

In performing OCP measurements in 1 M NaOH it was observed that the OCP of AZ31B experienced passivation reaching a potential of approximately -0.4 V$_{SCE}$ followed by breakdown reaching approximately -1.6 V$_{SCE}$. This fluctuation occurred in both short term (7 hours) and long term (120 hours) duration as seen in Figure 2.
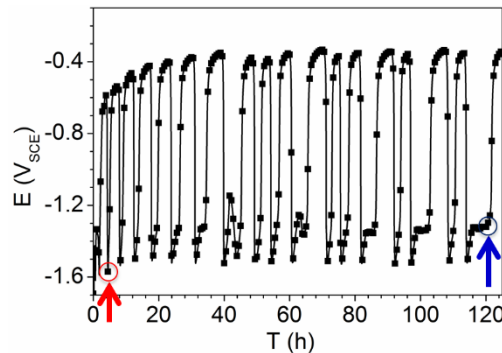

Figure 2: AZ31B OCP fluctuation.

In looking at the corrosion morphology for the short term test, it was observed that small Al-Mn IMPs completely dissolved, while the larger ones only partially dissolved (Figure 3a and b). In contrast, the Al-Zn particles did not dissolve (Figure 3c and d). In studying the surface of AZ31B, it was observed that a thick oxide film developed on the α-Mg matrix, but neither on the Al-Zn particles nor β-phase (Figure 3e).
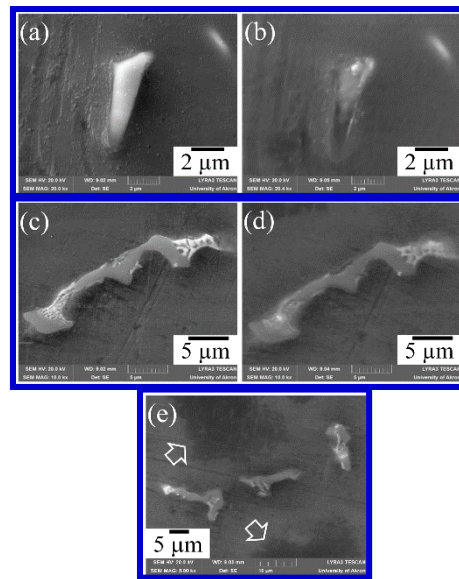

Figure 3: Corrosion morphology of IMPs for short term immersion in 1 M NaOH

Before performing a long term immersion test in 1 M NaOH and using the FE-SEM and the FIB the cross section of an Al-Mn particle was taken. It was observed that the Al-Mn particle had an elevated profile as compare to the α-Mg matrix as seen in Figure 4.

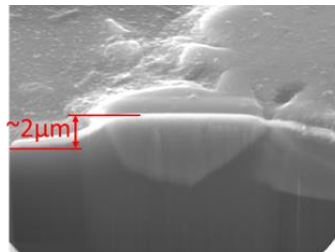Figure 4: Al-Mn IMP embedded within the α-Mg matrix and containing an elevated profile.

After the long term immersion test, the cross section of this Al-Mn IMP was taken (Figure 5a) and it was observed that it had partially dissolved and an oxide film developed on top of it which protected it from further dissolving (Figure 5b). A slight crack developed at the interface of the α-Mg matrix and the IMP as seen in Figure 5c. This crack may be responsible for the potential drops that were shown in Figure 2.
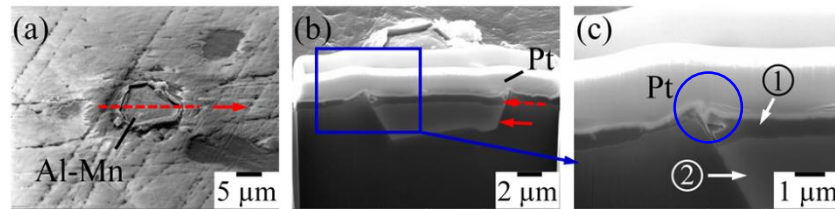

Figure 5: Cross section of Al-Mn IMP after immersion where a) shows the location of the cross section, b) shows the cross section of the IMP, and c) identifies a crack that developed during immersion.

In taking the cross section of the β-phase and the Al-Zn IMP, it was observed that a very thin oxide film had developed. The elemental compositions of the different sites located on Figures 5 and 6 are located on Table 2.
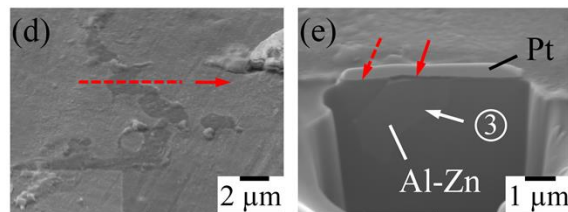

Figure 6: Cross section the Al-Zn IMP and the β-phase.

Table 2: Elemental compositions (at.%) of sites on Figures 5 and 6 indicating the oxide film and IMPs.

Site	O	Mg	Al	Mn	Zn	Fe
1	51.87	21.02	6.79	19.65	-	0.66
2	3.72	53.7	0.94	39.91	-	1.74
3	-	76.19	18.19	-	5.62	-

In studying the oxide film more closely, it was observed that oxide nodules formed at the interfaces of the α-Mg matrix and the β-phase. In taking the cross section, severe cracking was revealed on the α-Mg matrix side of the oxide nodule that had developed during the immersion. This crack could be responsible for the potential drops seen in Figure 2. The illustrations for this corrosion morphology can be seen in

Figure 7a, b, and c.

By taking the cross section of the α-Mg matrix that is away from the interface of α-Mg and β-phase, it was observed that a much thinner oxide film had developed as compared to that formed in the α-Mg and β-phase interface. Slight cracking due to dehydration that did not induce deep non-uniform oxidation within the matrix was also observed. These illustrations can be seen in Figure 7d, e, and f. The compositions of the sites indicated in Figure 7 can be seen in Table 3.
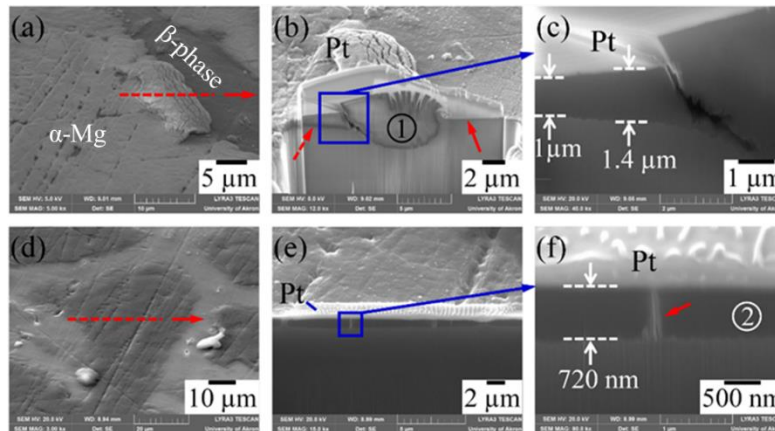

Figure 7: Study of the a) oxide nodule formation, b) the cross section of the oxide nodule, and c) severe cracking that develop. Study of the d) β-phase, e) the cross section, and f) cracking due to dehydration.

Table 3: Elemental compositions (at.%) on specific sites on Figure 7.

Site	O	Mg
1	36.42	63.58
2	32.8	67.2

The effects of oxygen were also studied on AZ31B in 1 M NaOH solution. Under deaerated conditions, the OCP stabilized around -1.3 V_{SCE} and still experienced potential drops. Under static conditions, it was seen that the OCP stabilized around -0.4 V_{SCE} with significant ~1V potential drops as seen in Figure 8.
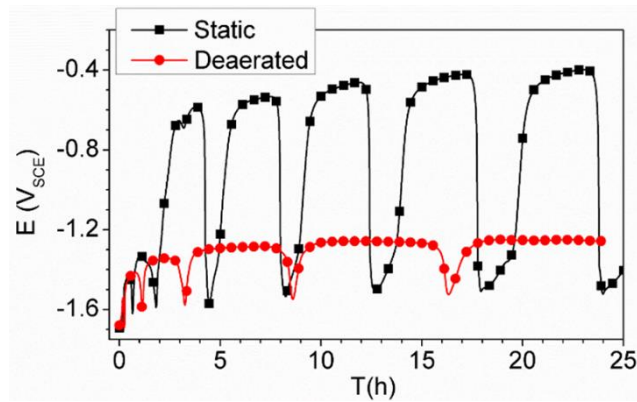
Figure 8: OCP profiles of AZ31B under static and deaerated conditions in 1 M NaOH.

In studying the corrosion morphology for AZ31B after being immersed in deaerated 1 M NaOH, it was observed that the Al-Mn particles dissolved due to the non-protective oxide film, which can be seen in Figure 9a and b. The oxide nodules that developed were sparse between the α-Mg matrix and the β-phase (Figure 9c). A thinner oxide film developed on the α-Mg matrix as compared static conditions. The elemental compositions for the sites indicated in Figure 9 can be seen in Table 4
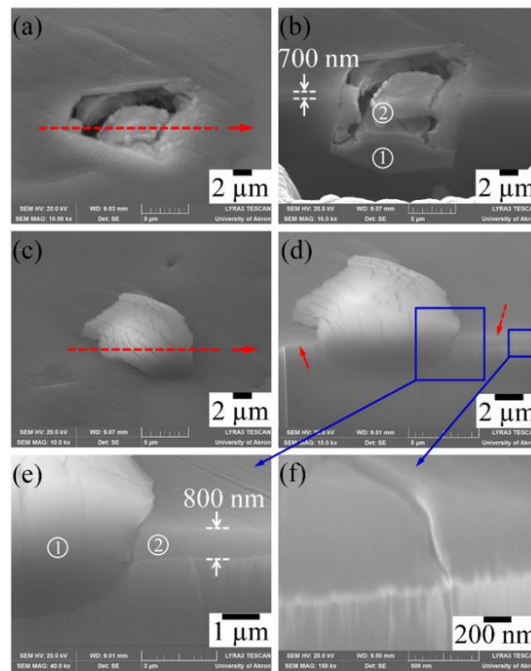
.

Figure 9: AZ31B a and b) Al-Mn IMP and c, d, e, and f) oxide nodule analysis under deaerated conditions.

Table 4: Elemental compositions (at.%) for sites indicated in Figure 9.

Site	O	Mg	Al	Ca	Cr	Mn	Fe
b1	0.1	33.6	1.77	-	-	60.2	4.37
b2	42.2	30.2	-	1.38	0.77	23.3	2.13
e1	43	56.7	0.03	0.11	-	0.14	0.03
e2	31.1	67.8	0.89	0.02	-	0.11	0.05

The effects of pH were also studied in this investigation as seen in Figure 10. OCP measurements were done at different pH levels and it was observed that significant potential rises and drops occurred in pH 13 and 14 however, these significant potential fluctuations did not occur in pH 10, 11, nor 12.
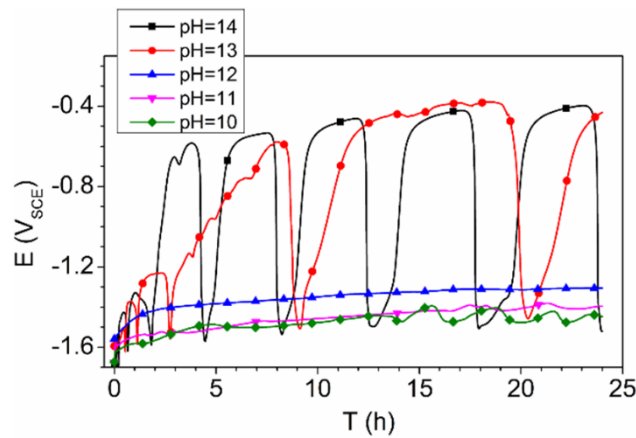

Figure 10: OCP measurements at different pH levels in static conditions.

By examining the corrosion morphology that occurred under these conditions, it was observed that at pH 10 and 11 there was severe corrosion and strong cathodic on the Al-Mn particles activities (marked by red arrows in Figure 11a and b). The cleanest surface, similar as the unexposed surface (Figure 11f), was seen under pH 12 conditions which indicates it had the least corrosion/passivation. In Figure 11 d and e, it can be seen that passivation increased from pH 13 to pH 14. The surface characterization seen in Figure 11 correlates well with the OCP measurements seen in Figure 10.
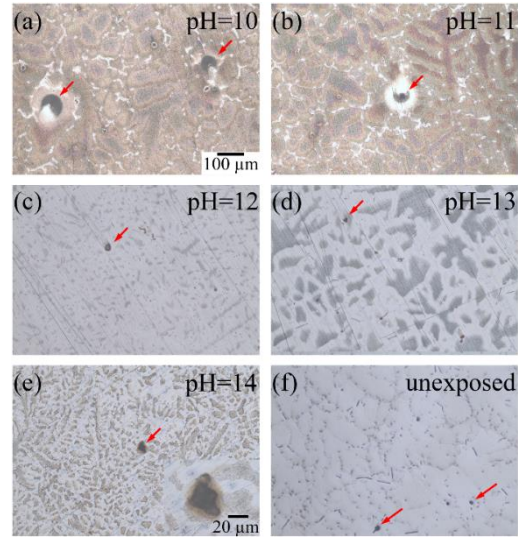
Figure 11: Corrosion morphology after being immersed at different pH levels. The 100 μm scale bar applies to images a – f.

Further investigation done for pH 11 corrosion morphology revealed oxide dome formations on top of Al-Mn particles (Figure 12a). The elevated profile of the Al-Mn IMP indicates that the Al-Mn particle did not dissolve and therefore, served as the cathodic sites (Figure 12c). The water reduction reaction produced OH^- ions that combined with the Mg^{2+} ions and formed this dome. Severe corrosion also occurred on the α-Mg matrix along with cracking (Figure 12d, e, and g) but not on the Al-Zn IMP (Figure 12h) and β-phase (Figure 12i). Table 5 shows the elemental compositions of the sites indicated in Figure 12.
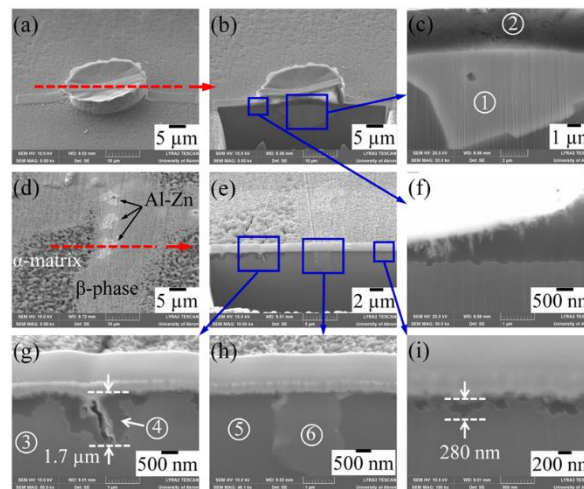

Figure 12: Oxide dome formation under static pH 11 conditions.

Table 5: Elemental compositions (at.%) of sites indicated on
Figure 12 for the IMP analysis of pH 11 under static
conditions.

Site	O	Mg	Al	Mn	Fe	Zn
1	-	30.7	6.5	59.6	3.3	-
2	60.5	39.5	-	-	-	-
3	-	100	-	-	-	-
4	14.6	85.4	-	-	-	-
5	-	94.8	5.2	-	-	-
6	-	80.8	10.3	-	-	8.9

Under pH 12 conditions, it was observed that a very thin passive film developed on the α-Mg matrix, β-phase, and both Al-Mn and Al-Zn IMPs (Figure 13). The elemental compositions identified on Figure 13 can be seen on Table 6.
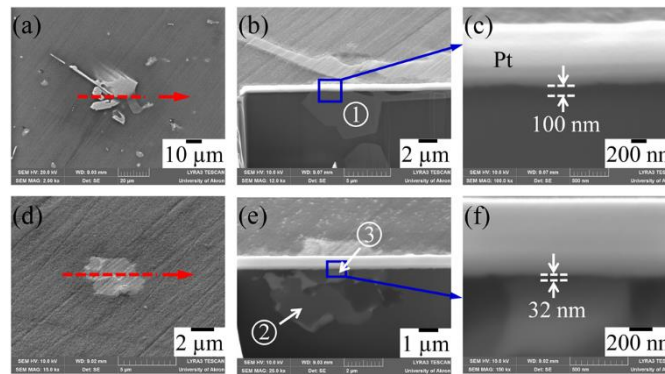

Figure 13: Corrosion morphology for AZ31B under pH 12 conditions.

Table 6: Elemental compositions (at.%) for sites indicated in Figure 13.

Site	O	Mg	Al	Mn	Zn
1	-	12.4	9.2	78.5	-
2	2.4	77.7	11.7	-	8.1
3	-	79.2	7.5	-	13.4

Cyclic potentiodynamic polarization was also done at different pH levels as seen in Figure 14. It was found that pH 12 had the lowest anodic current density. These results agree with the microscopic observations seen in Figure 11.
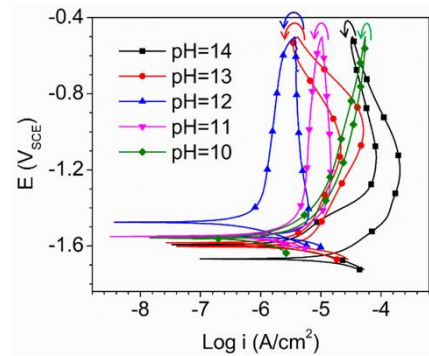

Figure 14: cyclic potentiodynamic polarization measurements done at different pH levels.

Cathodic activities occurring on AZ31B can be seen by bubble formations on the surface (Figure 15). Many hydrogen bubbles formed on the surface of AZ31B in pH 11 conditions. Very few bubbles formed under pH 12 conditions indicating less cathodic activity on the surface of AZ31B. The bubble formation under pH 13 and 14 conditions slowed with time indicating that the cathodic reaction transitioned from water reduction to oxygen reduction.
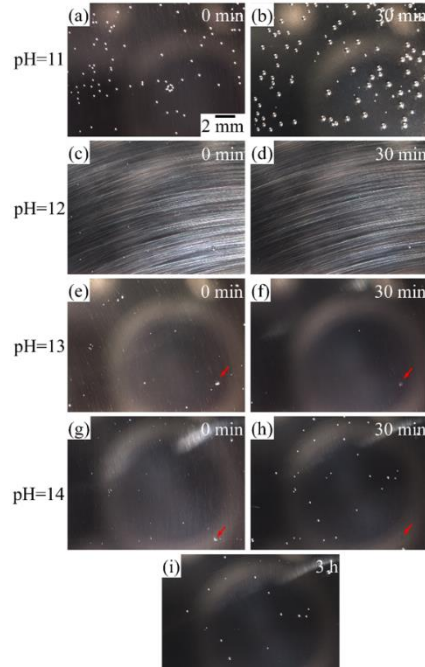
Figure 15: Bubble formations at different pH levels indicate cathodic activities on the surface of AZ31B.

SVET detected local cathodic currents originating from Al-Mn particles in pH 10 and 11 solutions as seen in Figure16a. No local currents could be detected at pH 12, 13, or 14 as seen in Figure16 d as an example shown in Figure 16d. The elemental compositions for the sites indicated in Figure 16c can be seen in Table 7.
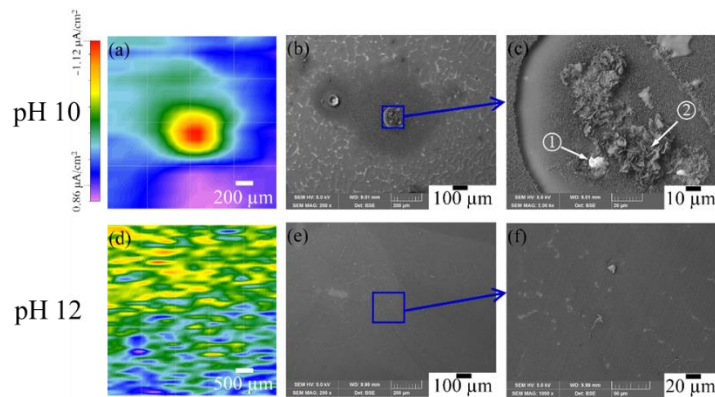

Figure 16: Cathodic currents were detected for pH 10, but not for pH 12 and above.

Discussion/Analysis

The results gathered above indicate that under different environments AZ31B behaves differently. AZ31B secondary phases and IMPs took on different roles depending on the conditions that they were placed

under. Oxygen is one of factors that played a part in the passivation of the Mg alloy. Under static conditions, various large oxide modules were found at the interface of the α-Mg matrix and the β-phase due to the galvanic coupling effects that are occurring at these locations. The α-Mg matrix is acting as the anodic site, while the β-phase and the Al-Zn particles are the cathodic sites supporting the cathodic reactions. As the passive film forms and thickens, the large change in volume causes an increase in stress and leads to cracking. The crack exposes Mg within the α-Mg matrix and allows for solution to penetrate through the crack. This leads to the oxidation of the Mg and the oxide nodule becomes embedded in the alloy. This process is depicted in Figure 17.
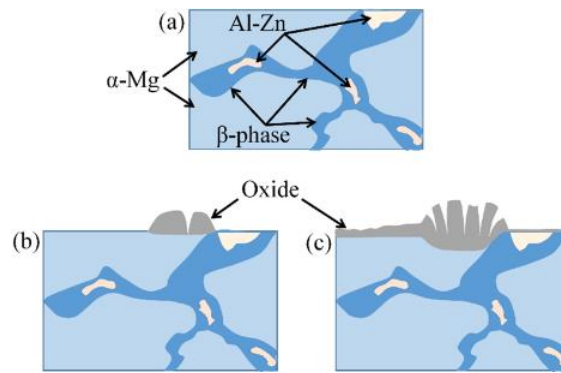

Figure 17: Oxide nodule formation mechanism.

From Figure 8, it was clear that the oxygen reduction reaction was responsible for the potential rise reaching -0.4 V_{SCE}. The frequency of the potential drops also decreased under deaerated conditions as compared to static conditions. Oxide nodule formation also became sparse due to the lack of oxygen and the Al-Mn IMPs dissolved due to the lack of protection.

The pH of the solution was another factor that effected what role the secondary phases and IMPs played within AZ31B. At pH 10 and 11, the Al-Mn IMPs did not dissolve. Figures 12a and b displays an Al-Mn IMP that maintained its elevated profile and was covered by an oxide dome indicating that the IMP was the cathodic site in this environment. The cathodic nature of this IMP supports the cathodic reactions which produce H_2 bubbles on top of the Al-Mn IMP.
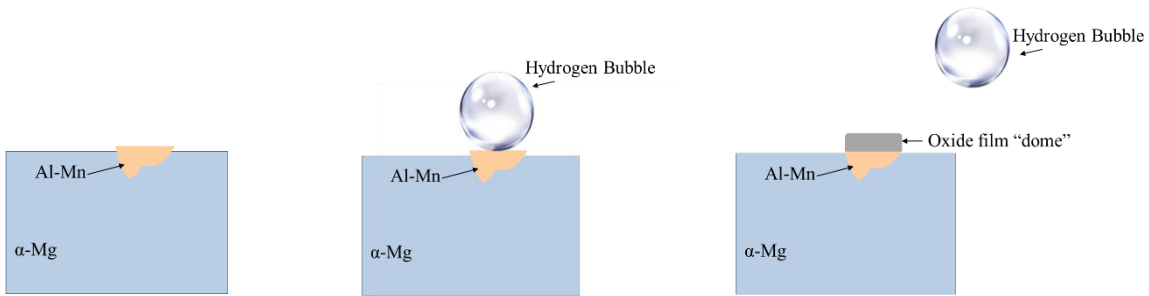
Figure 18: AZ31B passivation/corrosion behavior under pH 10 and 11 static conditions.

Solutions at pH 13 and 14 caused the Al-Mn IMPs to dissolve indicating their anodic nature. The adjacent α-Mg matrix then acts as the cathode in these conditions. From these results, it can be deduced that the bubbles form at the interface of the Al-Mn IMP and the α-Mg matrix. The Al-Mn IMP dissolves and is then protected from dissolving any further by an oxide film.
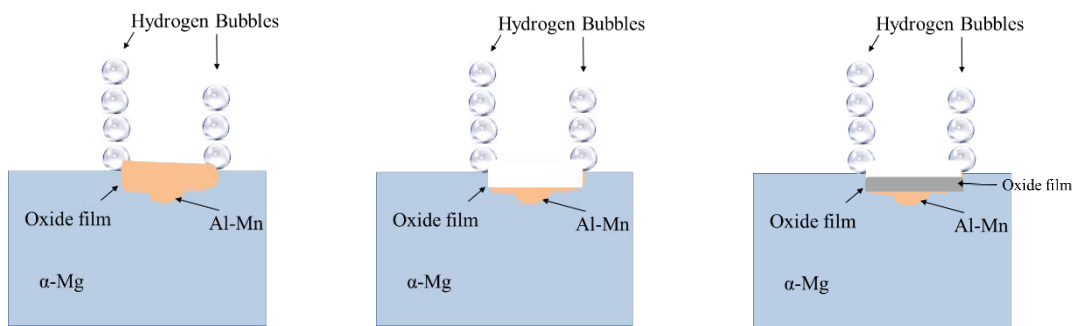

Figure 19: AZ31B passivation/corrosion behavior under pH 13 and 14 static conditions.

From this study, it was obtained that the secondary phases and IMPs within AZ31B can undergo different properties and be a result of the potential fluctuation as a result of galvanic coupling.

Literature Cited

[1] Jilani. "Difference Between Aluminum and Magnesium." DifferenceBetween.net. April 15, 2010

http://www.differencebetween.net/object/difference-between-aluminum-and-magnesium/.

[2] P.F. King, Magnesium as a Passive Metal, J. Electrochem. Soc. 110 (1963) 1113.

doi:10.1149/1.2425600.

[3] Taheri, J.R. Kish, Nature of Surface Film Formed on Mg Exposed to 1 M naOH, J. Electrochem. Soc.

160 (2012) C36-C41. doi: 10.1149/2.018302jes.